Turbulent Dynamo Action in Binary Neutron Star Mergers

Eduardo M. Gutiérrez
Postdoctoral Scholar
Penn State University

With: D. Radice (PSU), J. Fields (IAS), J. Stone (IAS)

arXiv:2601.20953

4th February 2026
YITP long-term workshop
Kyoto, Japan

PennState
Eberly College of Science

Why do magnetic fields matter in binary neutron star mergers?

- Key role in the launching of **MHD winds**, **relativistic jets**, **sGRBs**, **precursors or delayed emission**, **kilonova**

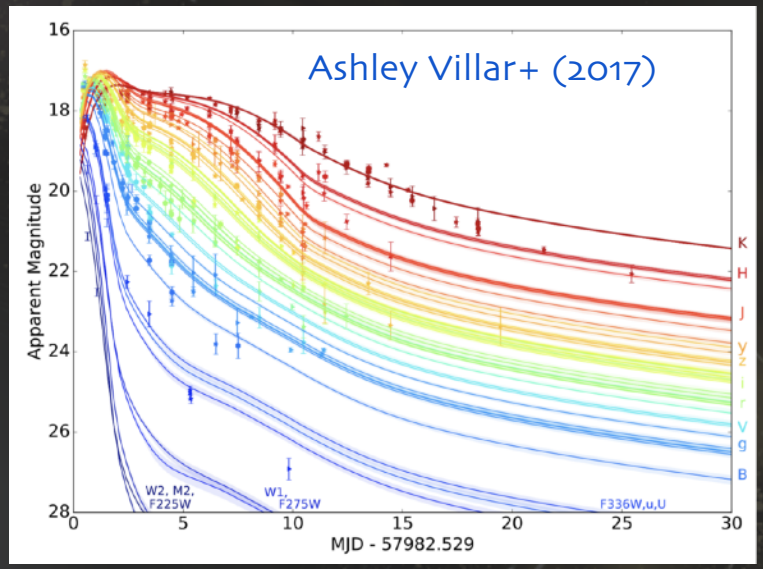

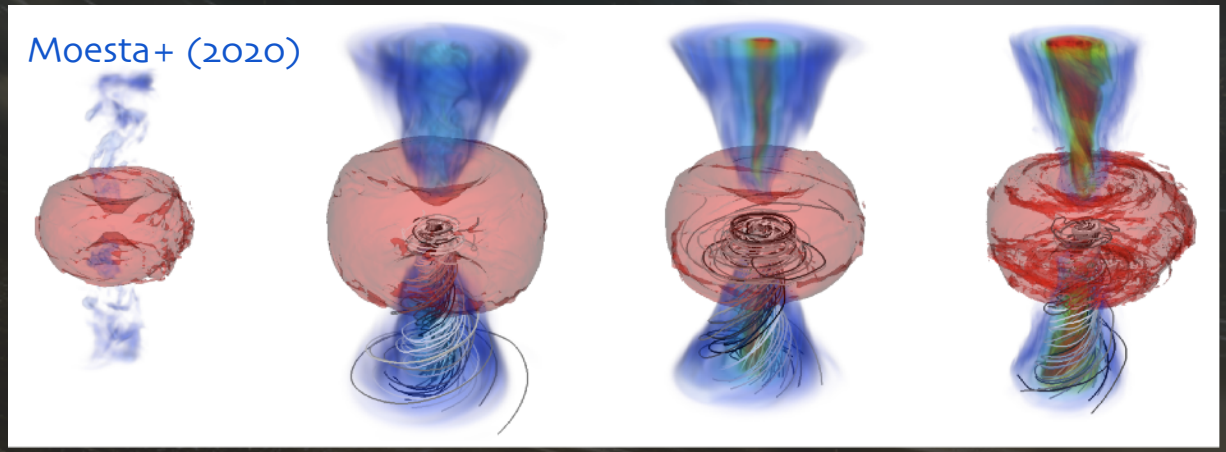

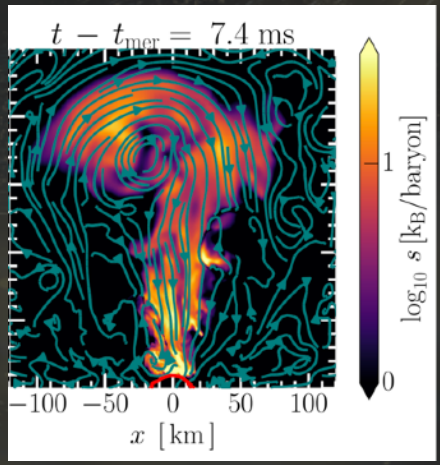

Most & Quataert (2023)

Why do magnetic fields matter in binary neutron star mergers?

- Binary NSs: $B_{\rm surf} \sim 10^8 - 10^{12}$ G

Lorimer (2008)

$$E_B \sim 5 \times 10^{41} B_{12} \text{ erg}$$

$$\ll E_k \sim 10^{53} \text{ erg}$$

- During and after the merger, **instabilities can amplify the magnetic field** by ~orders of magnitude.

$$E_B \sim 10^{51} \text{ erg}$$

$$B \gtrsim 10^{16} \text{ G}$$

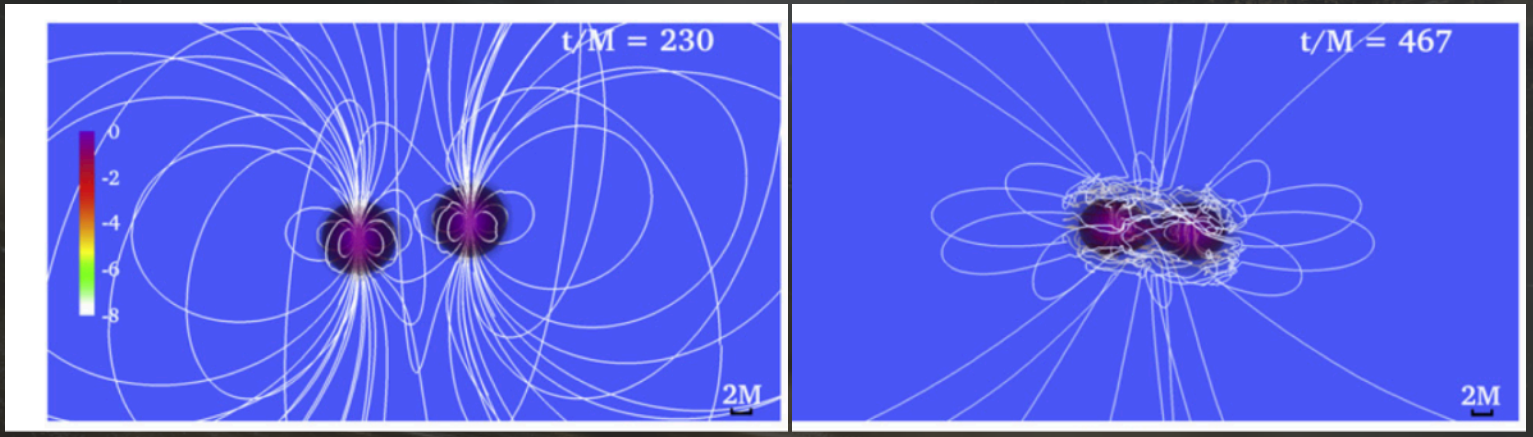

Instabilities drive dynamo processes that amplify the magnetic field

- Kelvin-Helmholtz Instability (KHI)
  Price & Rosswog (2006); Obergaulinger+2010; Zrake & MacFadyen (2013); Giacomazzo+2015; Kiuchi+2014,2015;…
- MRI-driven dynamo, winding
  Siegel+2013; Kiuchi+2024; Most (2023); Reboul-Salze+2025; Aguilera-Miret+2025;…
- Tayler-Spruit dynamo
  Reboul-Salze+2024
- …

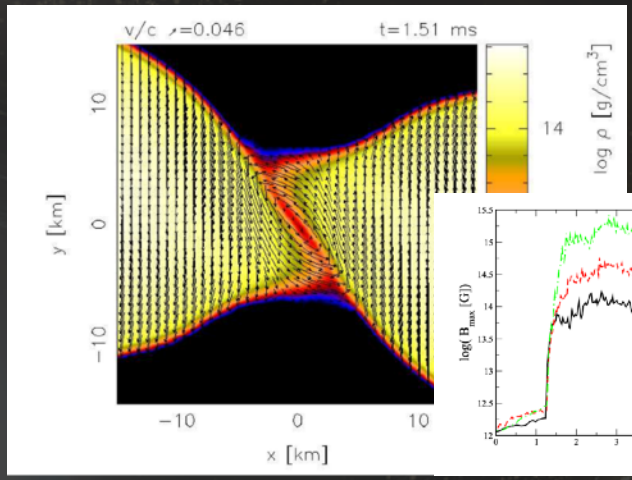

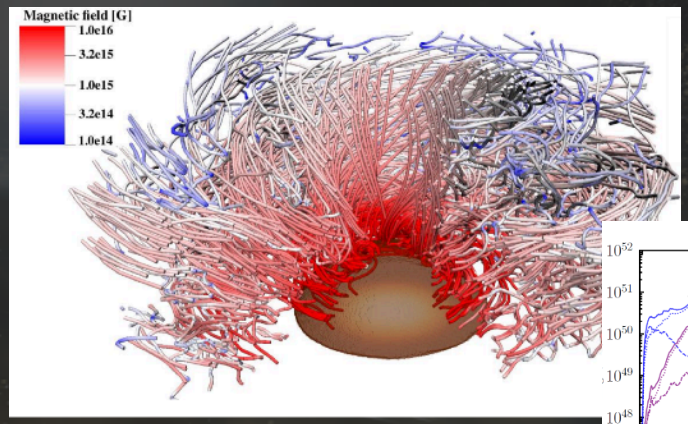

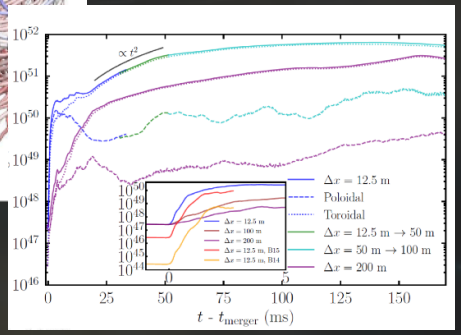

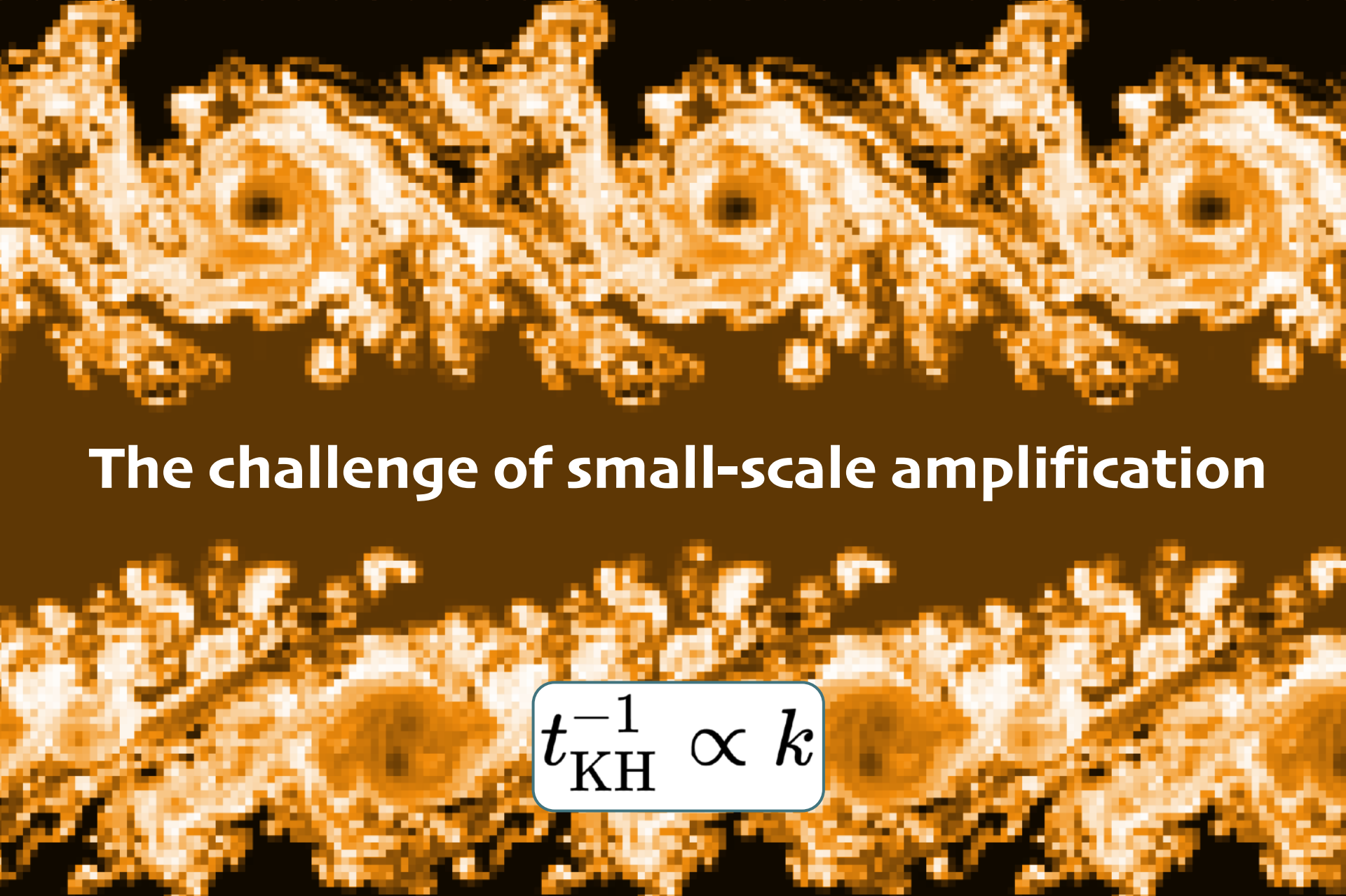
The challenge of small-scale amplification
$t_{\mathrm{KH}}^{-1} \propto k$

How to capture the large magnetic field amplification due to the KHI after merger in numerical simulations?

- High resolution
- Sub-grid modeling
- Initialize artificially large magnetic fields

Kiuchi+ (2014, 2015, 2023, 2024), Ciolfi+ (2019, 2020), Palenzuela+ (2022), Aguilera-Miret+ (2022, 2023), Chabanov+ (2023), Combi & Siegel (2023), Ruiz+ (2011, 2016, 2020, 2021), Kawamura+ (2016);…

We investigate the KHI amplification by means of a "zoom-in" simulation approach

FIRST: We run a global simulation of BNS merger using AthenaK:

- SFHo EOS (w/ trapped ν)
- $M_1 = M_1 = 1.3 M_\odot$
- $B_{\rm surf} \sim 10^{10}$ G
- $\Delta x \approx 92$ m
- $$\mathcal{A}_\phi = \frac{\pi r_0^2 I_0 \varpi^2}{\left(r_0^2 + r^2\right)^{3/2}} \left[1 + \frac{15 r_0^2 (r_0^2 + \varpi^2)}{8\left(r_0^2 + r^2\right)^2}\right]$$

Global simulation evolved up to a few milliseconds after the merger. We record high-frequency data in the inner regions

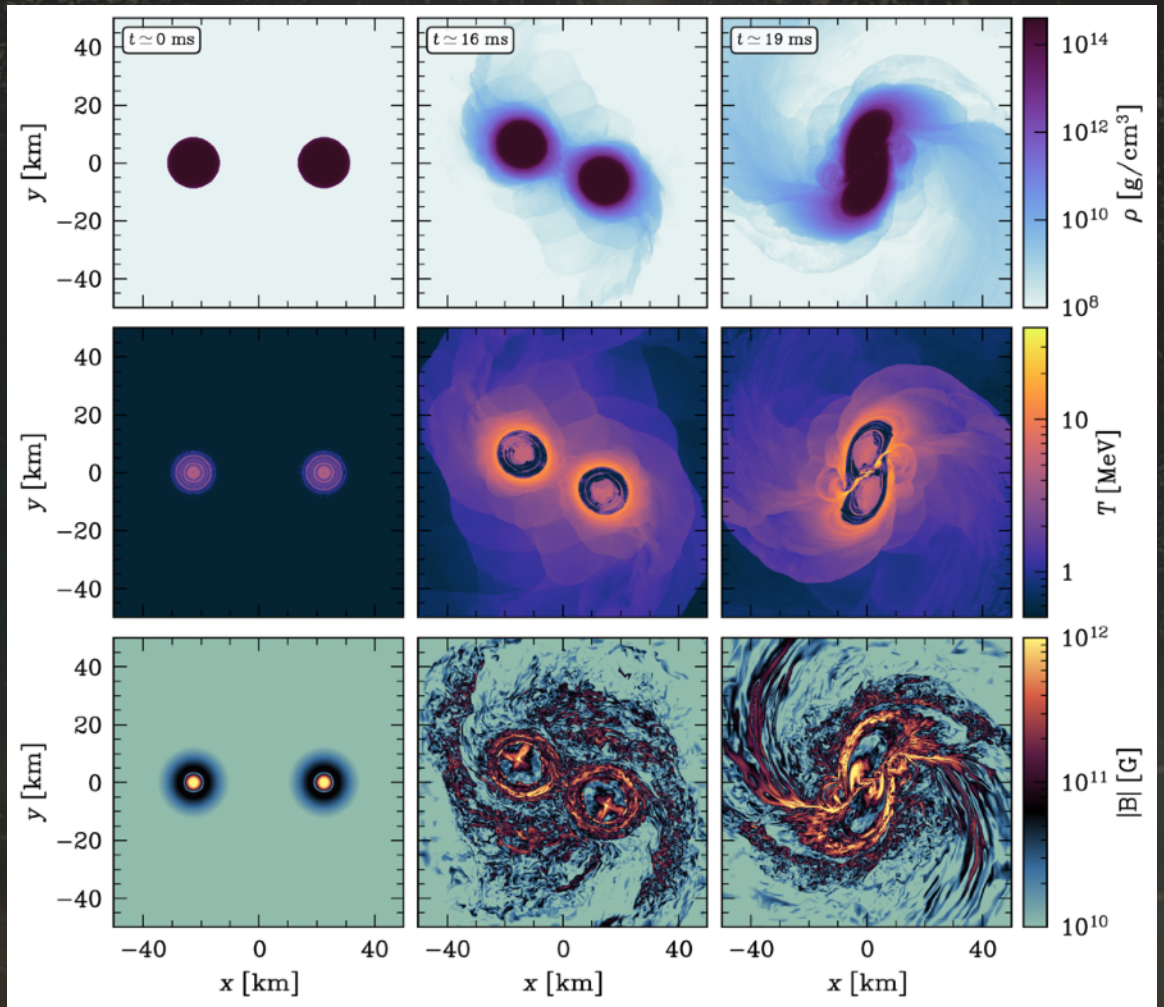

THEN: **when the stars make contact, we map the region containing the hot shear-layer to a new "zoom-in" grid**

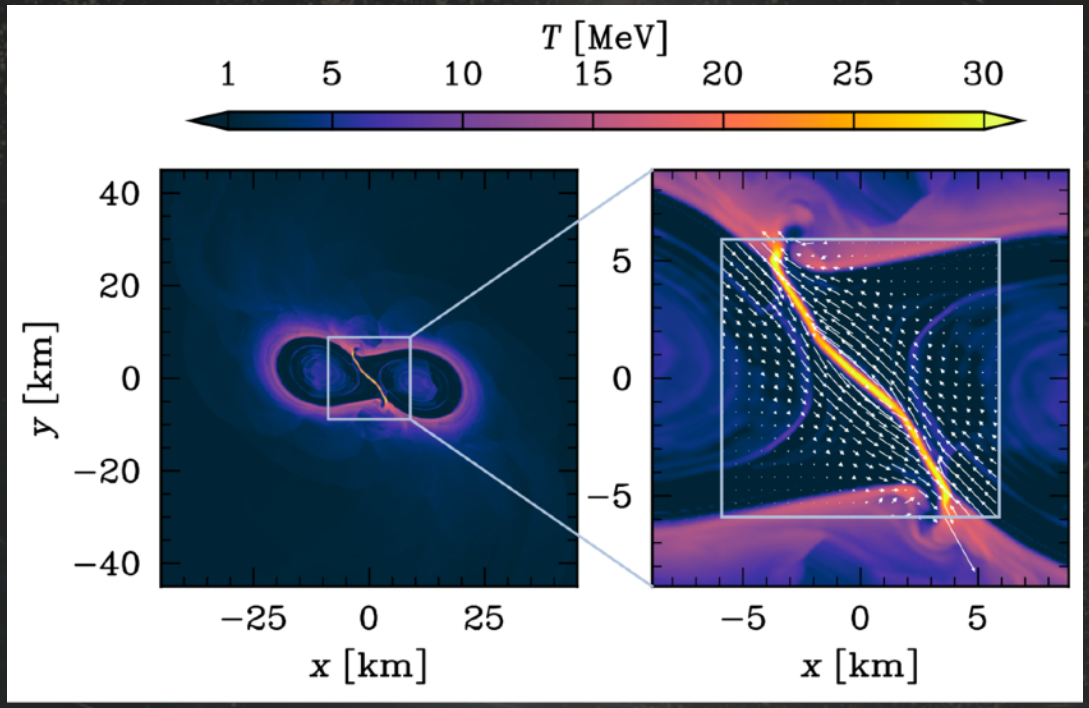

- We run a set of **"zoom-in"** simulations with resolutions:
  $\approx 92\text{m}, 46\text{m}, 23\text{m}, 12.5\text{m}, 5.8\text{m}, 2.9\text{m}$
- Width of shear layer is limited by the scale-height on the NS surface
  -> $h \sim (\rho/\partial_r \rho) \sim (50 - 100)$ m: **gravity introduces a length scale**.


t = 0.00 ms

The shear layer rapidly becomes KHI-unstable and generates vortical structures where the field undergoes exponential amplification.

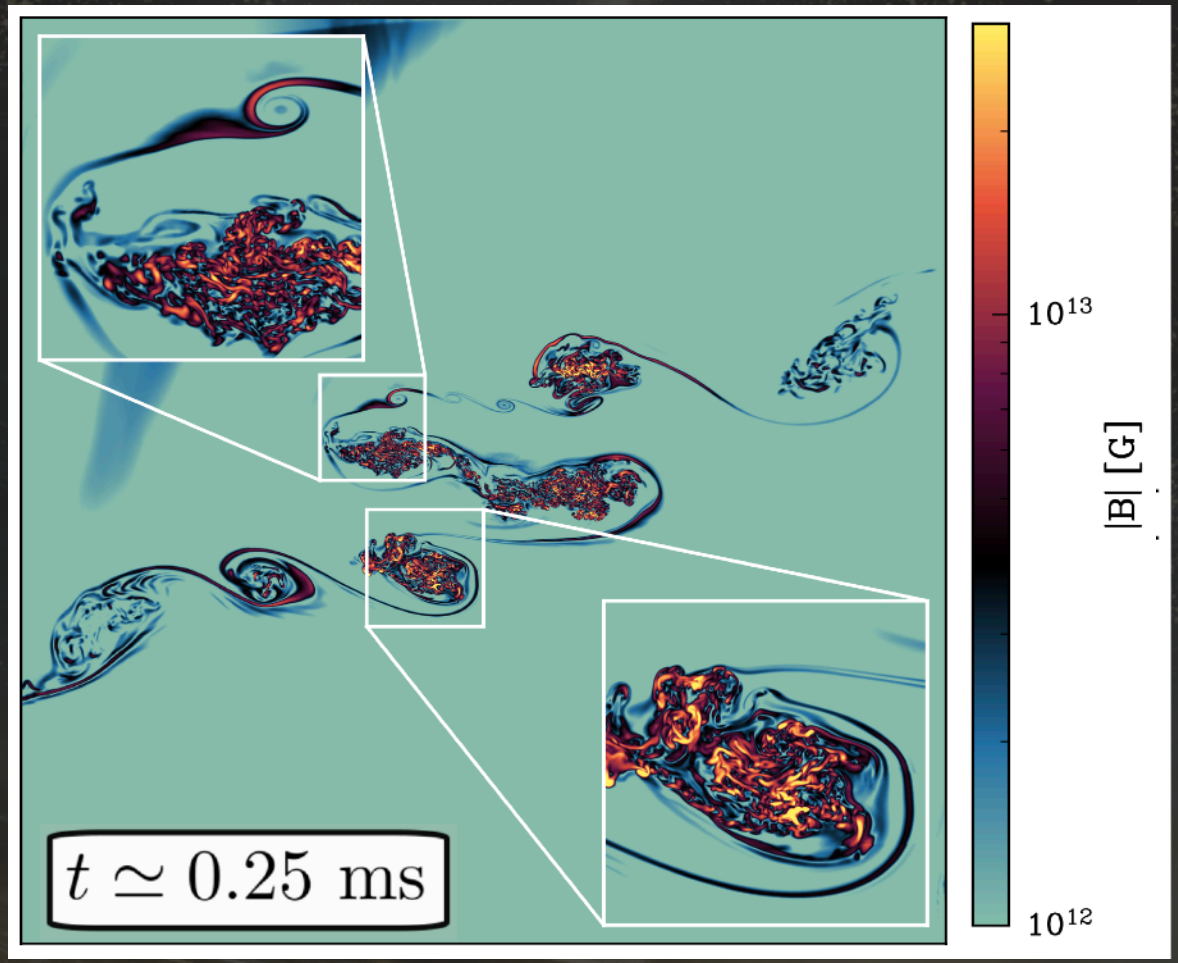

As vortices becomes themselves KHI-unstable, the shear layer grows in size, merge, and fill a large fraction of the volume with turbulent structures.

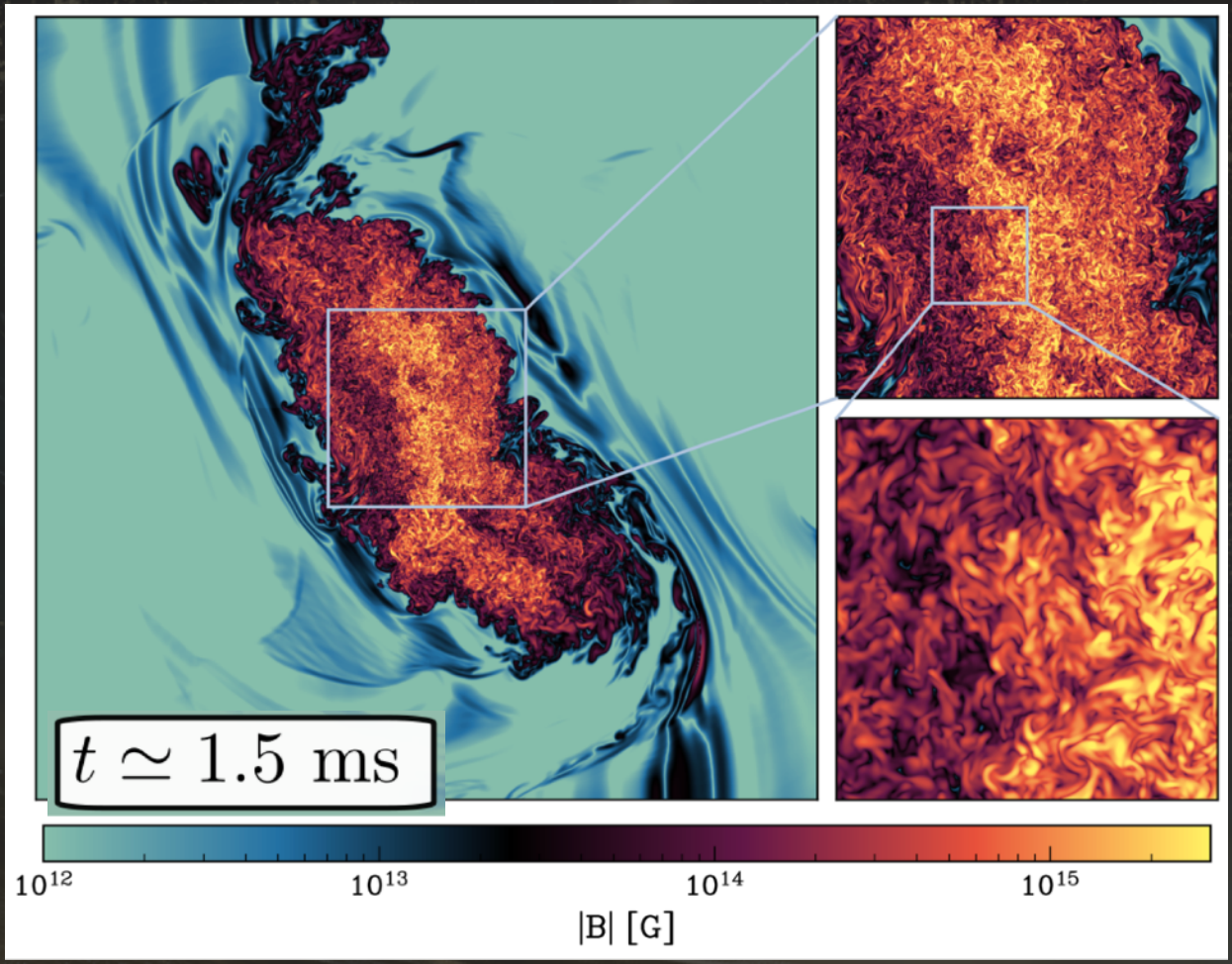

The velocity power spectrum rapidly develops a Kolmogorov power spectrum

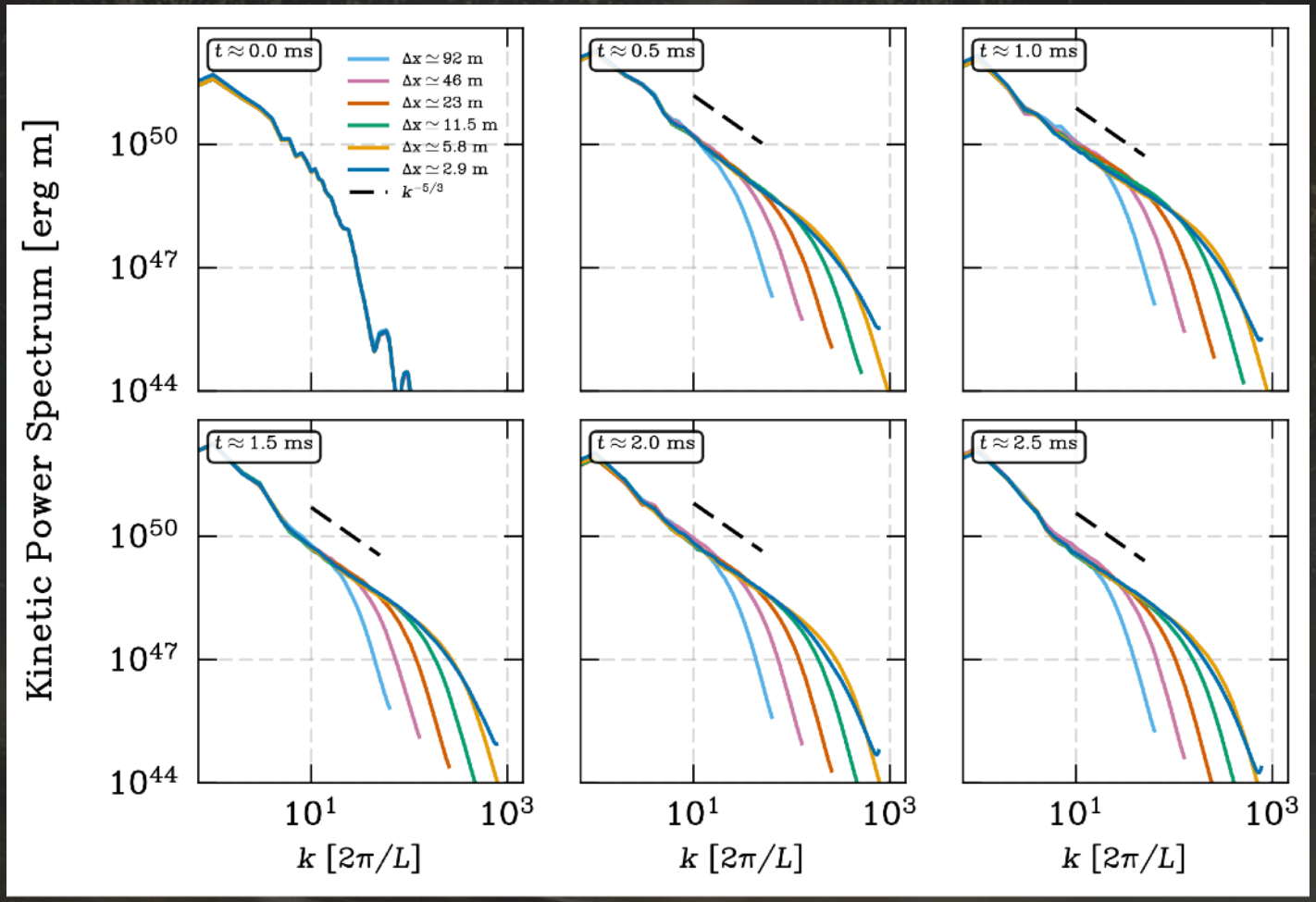

Magnetic spectrum suffers small-scale amplification; develops a Kazantsev power spectrum. At later times, magnetic field begins to grow on large scales

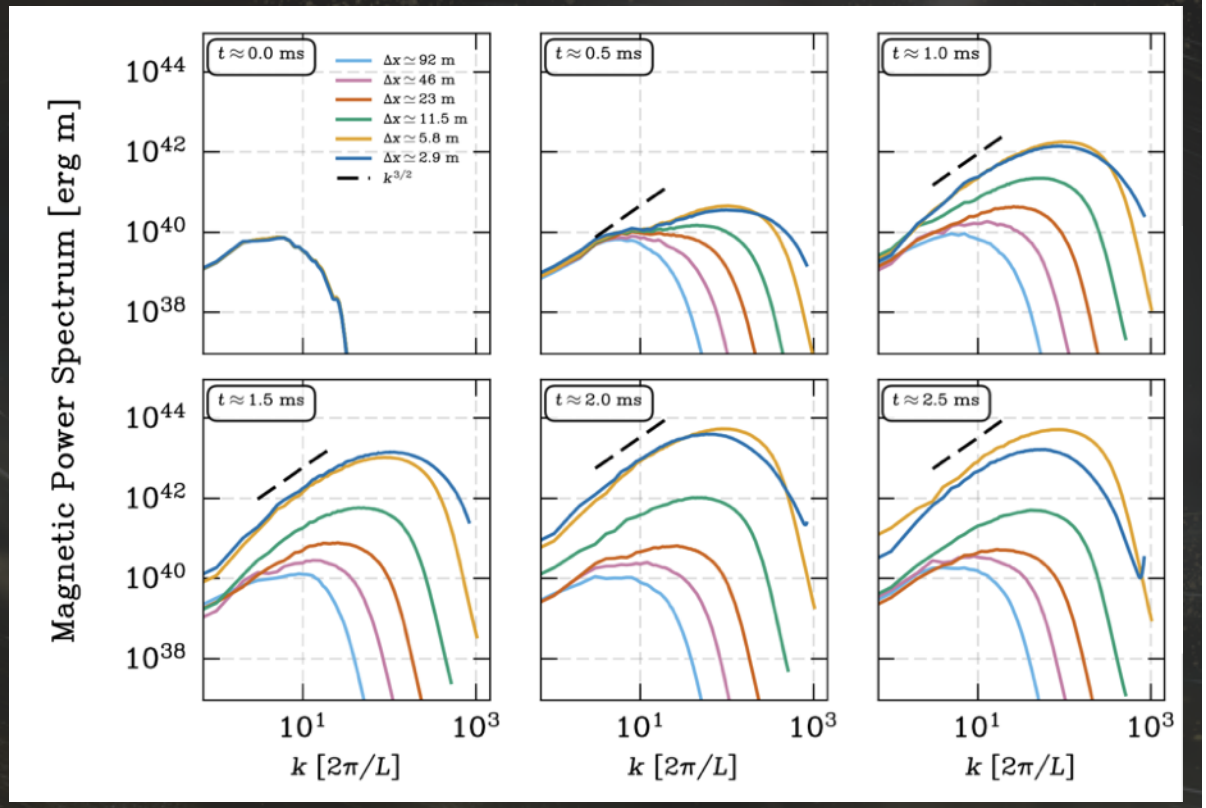

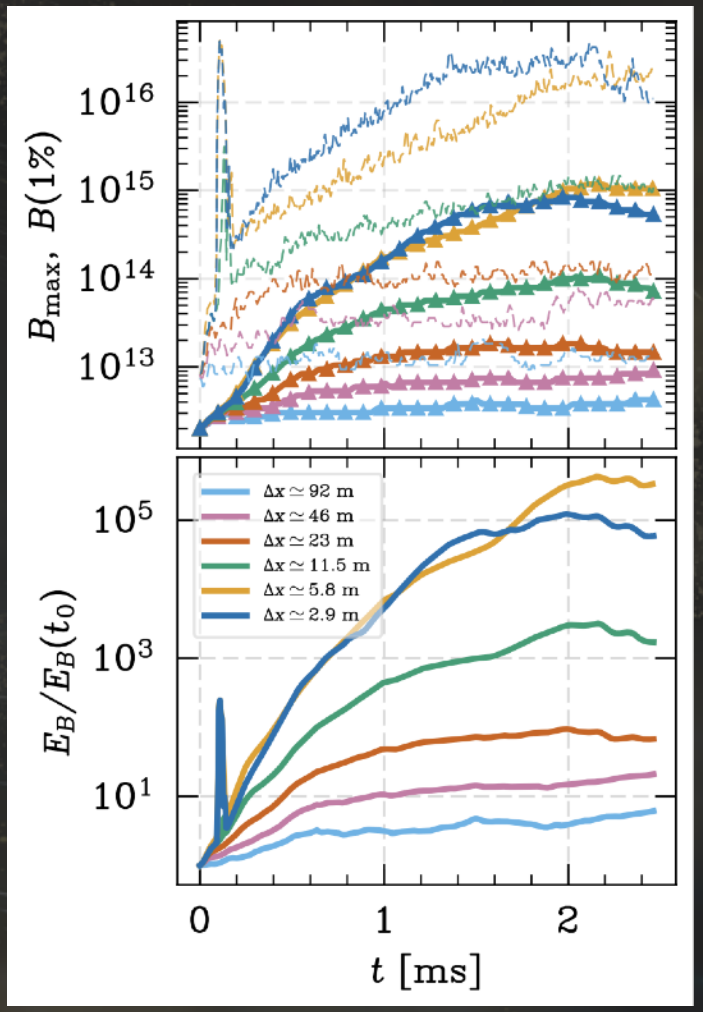

Magnetic power at progressively lower wavenumbers begins to increase, after the small-scale field has reached sufficiently large amplitudes

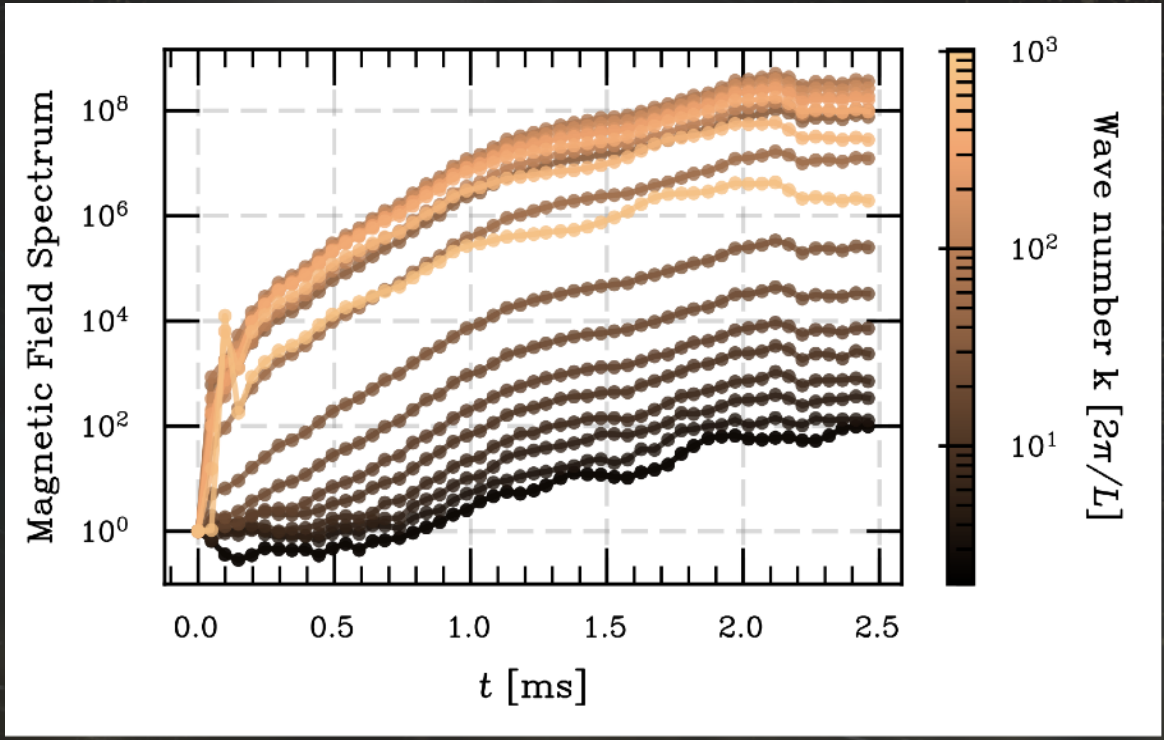

Takeaways

- KHI in BNS mergers acts as a turbulent dynamo.
- Magnetar-level fields within milliseconds.
- Growth at large-scales
- Breakout? Potential to powering gamma-ray flares

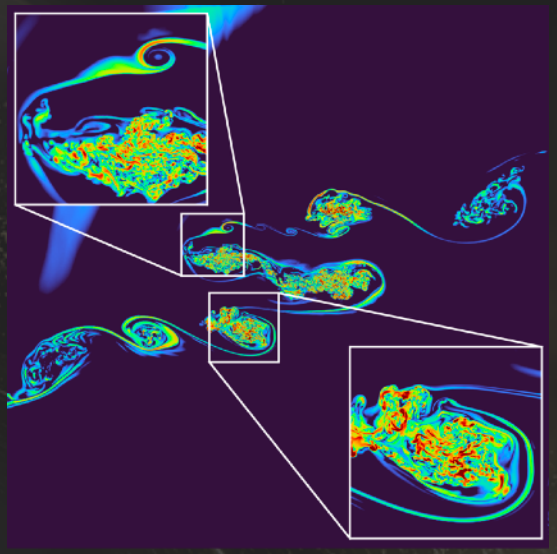

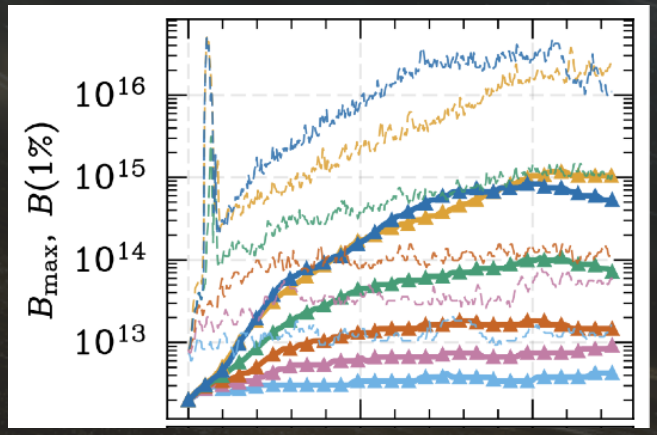

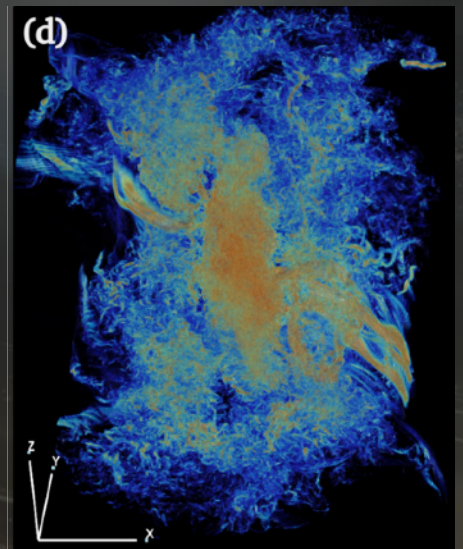

arXiv:2601.20953

Backup slides

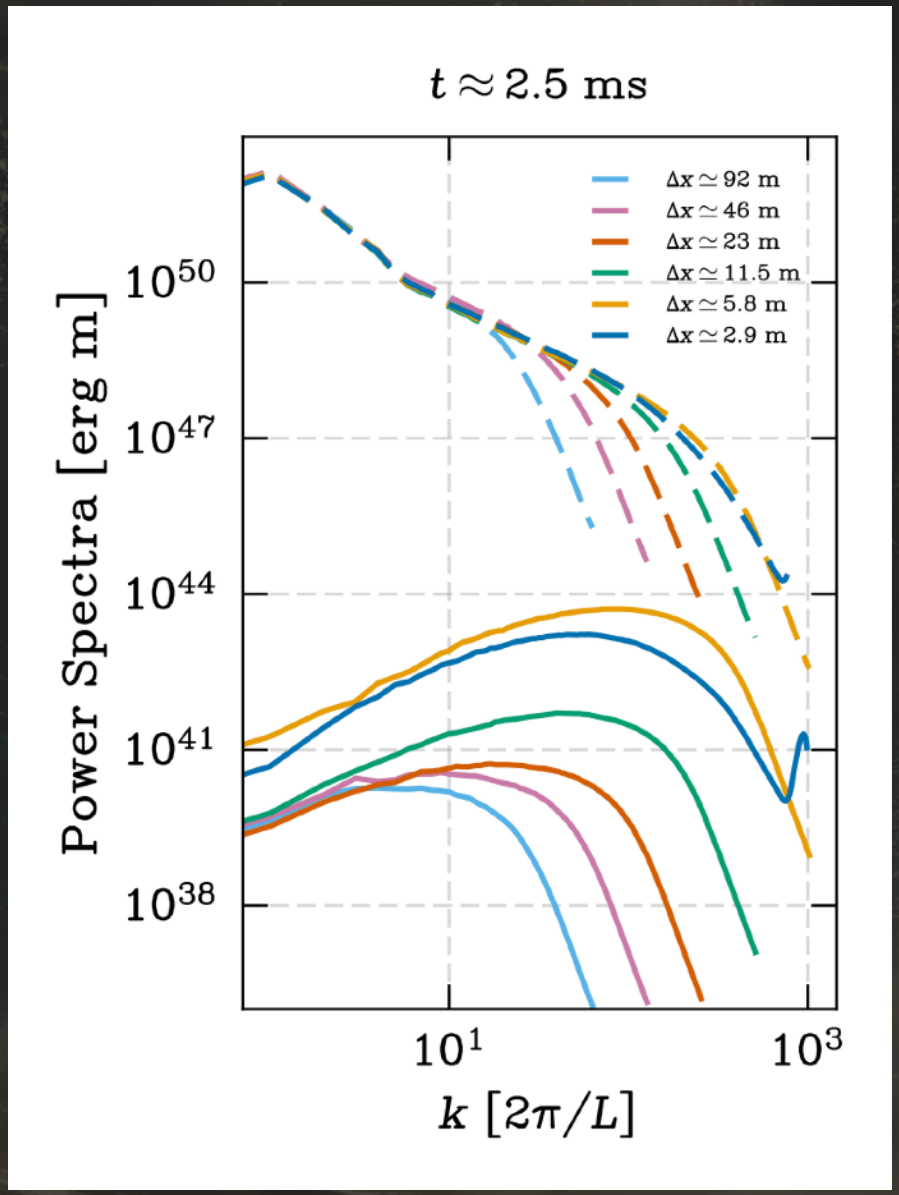
$t \approx 2.5$ ms
$\Delta x \simeq 92$ m
$\Delta x \simeq 46$ m
$\Delta x \simeq 23$ m
$\Delta x \simeq 11.5$ m
$\Delta x \simeq 5.8$ m
$\Delta x \simeq 2.9$ m
Power Spectra [erg m]
10^{50}
10^{47}
10^{44}
10^{41}
10^{38}
10^{1}
10^{3}
k $[2\pi/L]$

During the global simulation, we record simulation data in a cube of side length $2L$, $L = 4.5\ GM_\odot/c^2 \simeq 6.65$ km centered about the origin. This data is used to provide initial data, boundary conditions, and background metric for the zoom-in simulations. To avoid possible boundary effects, the domain of the zoom-in simulations is restricted to a smaller cube with side length $2L'$, $L' = 4\ GM_\odot/c^2 \simeq 5.91$ km. The data is stored on a Chebyshev endpoint grid with $N = 64$ points in each direction and sampled with a frequency of $\Delta t = 0.09375\ GM_\odot/c^3 \simeq 0.46\ \mu$s. In particular, we store and interpolate the fluid baryon number density n_b, the Lorentz-factor-weighted three velocity $\tilde{v}^i = Wv^i$, W being the Lorentz factor, the pressure p, and the proton fraction Y_e of the plasma. The spacetime geometry is encoded in the lapse and shift vectors α and β^i, respectively, the three metric γ_{ik}, and the extrinsic curvature, K_{ik}. See, e.g., Ref. [53] for a definition of these

We interpolate all fields, except for the magnetic field (which is described in detail below), using 6th order Lagrange interpolation on the Chebyshev grid. This results in a speedup of a factor $\sim(N/5)^3 \simeq 2 \times 10^3$ compared to the direct evaluation of the Chebyshev collocation basis, which would have been prohibitively expensive, as we need to interpolate spacetime data and boundary conditions at each timestep of the zoom-in simulation. We have verified that the error introduced by this truncation of the interpolation stencil is negligible, as

Still, unphysical artifacts can be expected if the initial magnetic field is not solenoidal. As a first step, we reconstruct the vector potential using the identity [55]

$$\mathcal{A}_i(x) = \int_0^1 \epsilon_{ijk}\, \mathcal{B}^j(\lambda x)\, x^k\, \lambda\, \mathrm{d}\lambda\,, \tag{2}$$

where ϵ_{ijk} is the antisymmetric symbol with $\epsilon_{123} = 1$. The integral in Eq. (2) is computed in pre-processing for each grid point using a Gaussian quadrature with 12 points. To this aim, the $\mathcal{B}$ field data is interpolated to the quadrature points using a 10th order accurate Lagrange interpolation.

Next, we interpolate the vector potential $\mathcal{A}_i$ at the cell edges of the zoom-in grid, using the same 6th order interpolation approach as for the other variables, and evaluate

$$\mathcal{B}^i = \epsilon^{ijk}\, \partial_j\, \mathcal{A}_k \tag{3}$$

using the discrete curl operator consistent with the constrained-transport of `AthenaK`, e.g.,

$$\mathcal{B}^1_{k,j,i+1/2} = \frac{(\mathcal{A}_3)_{k,j+1/2,i+1/2} - (\mathcal{A}_3)_{k,j-1/2,i+1/2}}{\Delta x^2} - \frac{(\mathcal{A}_2)_{k+1/2,j,i+1/2} - (\mathcal{A}_2)_{k-1/2,j,i+1/2}}{\Delta x^3}\,, \tag{4}$$

Small, intermittent current sheets form. The current density traces B field gradients, showing where the field is stretched, twisted, and folded